Journal of Sound and Vibration (1997) **208**(5), 729–743

VIBRATION REDUCTION AND ISOLATION PERFORMANCE FOR ON–OFF CONTROL OF A FRICTION FORCE AT A SPRING SUPPORT

H. YAMAGUCHI AND M. YASHIMA

Department of Mechanical Engineering, *National Defense Academy*, *Hashirimizu* 1-10-20, *Yokosuka* 239, *Japan*

AND

Y. HIRAYAMA

National Defense Agency, 1-1, *Hatobamachi*, *Kobe*, *Japan*

(*Received* 20 *January* 1997, *and in final form* 3 *July* 1997)

In order to isolate the vibration transmitted to machines or structures from a floor and to reduce vibration caused by a shock force applied directly to them, a new method of on–off control for the spring support is presented in this paper. The suspension system includes the auxiliary spring and brake mechanism that are designed to control the clamping friction force at the end of the spring. The clamping friction force is varied according to the switching law, which is deduced from the variable structure systems (VSS) control theory. The switching law takes into account the energy dissipation due to friction. In the numerical simulations, the performance of the impulse response reduction and the displacement transmissibility is investigated. The results show that the method is effective in suppressing shock motion and isolating vibration.

1. INTRODUCTION

Vibration reduction and isolation to protect mechanical systems, vehicles and structures from the shock force and vibration environment present important and difficult problems. The conventional passive device composed of a spring and a damper suffers from inconsistent difficulties for these requirements, because the vibration caused by a shock force applied directly to the machine is reduced by increasing the spring stiffness and the damping, while the vibration transmitted from the floor is isolated by decreasing them. Therefore, the optimal spring stiffness and damping have been decided as a result of trade-off between these requirements, and the performance is limited. To overcome this limitation, active vibration control systems consisting of force and control devices that can generate forces based on state feedback have been the subject of extensive research efforts in recent years. Although active vibration control systems have high performance, they are more costly, more complex and less reliable than passive systems.

On the other hand, semi-active vibration control systems that vary the damping or stiffness properties of a passive element in response to the instantaneous states of motion compensate for the drawbacks of the active system. Hydraulic semi-active dampers with electromagnetically controlled valves have been investigated by many researchers and applied to vehicle suspensions [1–4]. Friction damping is also controlled by varying the force normal to a friction interface [5]. Several studies have investigated the effects of

0022–460X/97/500729 + 15 $25.00/0/sv971224

restoring force associated with stiffness term on vibration suppression of a flexible beam or a string subject to an axial force [6–8]. Recently, Yamaguchi *et al*. [9] proposed a suspension system with stiffness control based on the sliding mode of the variable structure systems (VSS) theory [10–12]. The stiffness-controllable spring is realized by varying the axial force for the two straight bars that are hinged to the mass in a line perpendicular to the direction of mass motion. Another type of stiffness control is the on–off control of the spring support clamping with the brake assembly. Onoda *et al*. [13] proposed the control logic, which changes two spring stiffness values depending on the state of mass motion by using the phase plane concept. However, the approach neglected the inertia of the stiffness member and assumed that the stiffness change was achieved instantaneously. To improve this impractical assumption, Warkentin and Semercigil [14] introduced the finite time duration during which the spring support remains unclamped, and investigated the effect on the transient response. They further showed that the time lag from the instant of peak displacement for the control action improves the performance of the system. However, the roles of the finite time duration and the time lag in the control logic have not been clarified theoretically. It is also noted that friction in the brake mechanism contributes to the damping and enhances the energy dissipation, although the effect of friction is not included in the analysis of Onoda *et al*. [13] and of Warkentin and Semercigil [14].

The purpose of this paper is to present a new method of on–off control for the spring support, in order to isolate vibration transmitted to machines or structures from the floor and to reduce vibration caused by a shock force applied directly to machines or structures. The suspension system includes the auxiliary spring and brake mechanism that are designed to control the clamping friction force at the end of the spring. The clamping force is varied according to the switching law, which is deduced from the VSS control theory taking account of the sliding mode. The switching law also takes into account the energy dissipation due to friction. The proposed method clarifies theoretically and develops the concept of control logic based on the phase plane proposed by Onoda *et al*. [13], and the roles of the finite time duration and time lag introduced by Warkentin and Semercigil [14]. In numerical simulations, the performance of the impulse response reduction and the displacement transmissibility is investigated. The results show that the method is effective in suppressing shock motion and isolating vibration.

2. SYSTEM MODEL OF ON–OFF SPRING SUPPORT CONTROL

The concept of on–off control of the spring support is idealized as shown in Figure 1. In Figure 1, the mass m supported by a spring of stiffness k_a is the main object to be reduced by vibration caused by the shock force applied directly or transmitted from the floor. The

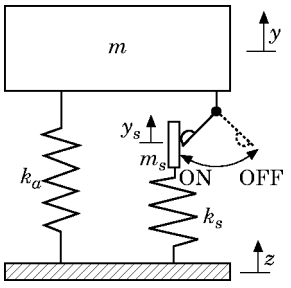

Figure 1. The system model.

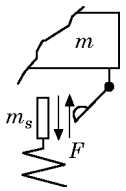

Figure 2. The friction force F at a joint.

auxiliary spring of stiffness k_s is employed to implement the control technique and is designed to control the upper end support by the joint switching device of mass m_s such as a brake mechanism. It is assumed that the mass m_s is much smaller than m and that the stiffness k_s is much larger than k_a. The state of motion is classified into three cases as follows: (A) the joint is not clamped (support off) and the masses m and m_s move freely of each other—in this case, the mass m is supported by the single spring of stiffness k_a; (B) the joint is clamped (support on) and the masses m and m_s are stuck together with no relative motion—in this case, the total mass of m and m_s is supported by two springs of stiffness k_a and k_s; (C) the joint is clamped (support on), but the relative motion between the masses m and m_s occurs owing to interfacial slip. This is a single-degree-of-freedom system with no energy dissipation for both cases (A) and (B), although the natural frequencies are different. On the other hand, the system becomes complicated and the energy is dissipated due to friction damping during slip for case (C).

Equation of motion for case (C) is given by

$$m(\mathrm{d}^2y/\mathrm{d}t^2) = -k_a(y - z) + F, \tag{1}$$

$$m_s(\mathrm{d}^2r/\mathrm{d}t^2) = -k_s(r + y - z) - F - m_s(\mathrm{d}^2y/\mathrm{d}t^2), \tag{2}$$

where y and z are the displacements of mass m and floor, respectively, r is the relative displacement, t is time, and F is the interfacial friction force between masses m and m_s, as shown in Figure 2. The relative displacement is defined by

$$r = y_s - y, \tag{3}$$

where y_s is the displacement of mass m_s. For conciseness, the friction force F is given by Coulomb's law, abbreviated as

$$F = \mathrm{sgn}\,(\mathrm{d}r/\mathrm{d}t)F_s, \tag{4}$$

where sgn is the sign function, defined to be $+1$ or -1 depending on whether its argument is positive or negative, and F_s is the magnitude of the constant friction force during slip.

The equation of motion for case (A) is also expressed by equations (1) and (2), setting $F = 0$. On the other hand, the relative displacement r is kept constant for case (B). In this case, we eliminate F from equations (1) and (2) and obtain

$$(m + m_s)(\mathrm{d}^2y/\mathrm{d}t^2) = -(k_a + k_s)(y - z) - k_sr_s \tag{5}$$

where r_s is the relative displacement at the moment when masses m and m_s are touching. It is noted that $\mathrm{d}^2r/\mathrm{d}t^2 = 0$ when masses m and m_s are touching. Then, the friction force F is obtained from equation (2):

$$F = -k_s(r_s + y - z) - m_s(\mathrm{d}^2y/\mathrm{d}t^2). \tag{6}$$

The two masses continue to be touching if the friction force given by equation (6) does not exceed the magnitude of constant friction force during slip, i.e.,

$$|-k_s(r_s + y - z) - m_s(\mathrm{d}^2y/\mathrm{d}t^2)| < F_s. \tag{7}$$

The relative motion between the masses occurs again if the condition of equation (7) is not satisfied.

3. CONTROL LAW CONSIDERATIONS

For a general expression, we introduce the non-dimensional values

$$\begin{gathered}\bar{y} = y/\delta_{st}, \qquad \bar{r} = r/\delta_{st}, \qquad \bar{r}_s = r_s/\delta_{st}, \qquad \bar{z} = z/\delta_{st}, \\ \tau = \Omega_0 t/2\pi, \qquad \bar{F} = F/mg, \qquad \bar{F}_s = F_s/mg\end{gathered} \tag{8}$$

and define the mass ratio λ and the spring stiffness ratio v:

$$\lambda = m_s/m, \qquad v^2 = (k_s/m_s)/\Omega_0^2, \tag{9}$$

where

$$\Omega_0^2 = k_a/m, \qquad \delta_{st} = g/\Omega_0^2 \tag{10}$$

and g is the gravitational acceleration constant.

Then, the solution of equation (5) leads to

$$\bar{v}^2 + a(\bar{y} - \beta)^2 = D \tag{11}$$

where D is a constant to be determined by the initial conditions, and

$$\bar{v} = \mathrm{d}\bar{y}/\mathrm{d}\tau, \qquad \beta = \bar{z} - \lambda v^2 \bar{r}_s/(1 + \lambda v^2), \qquad a = 4\pi^2(1 + \lambda v^2)/(1 + \lambda). \tag{12}$$

Equation (11) indicates that the motion of mass m for case (B) is described by an elliptic trajectory with center $(\beta, 0)$ in the $\bar{y}$–$\bar{v}$ phase plane. It is noted that β depends on $\bar{z}$ and $\bar{r}_s$. Since the floor displacement $\bar{z}$ varies with time in general, in practice the trajectory is no longer an ellipse. Nevertheless, the trajectory is controlled by the relative displacement $\bar{r}_s$, if $\bar{r}_s$ is shifted much more than the variation of $\bar{z}$. In Figure 3, ellipses denoted by the single-dotted and broken lines are the example of trajectories when $\bar{r}_s$ is kept near maximum and minimum so that β is kept near the minimum and the maximum, respectively. Here, the floor displacement is taken as zero ($\bar{z} = 0$).

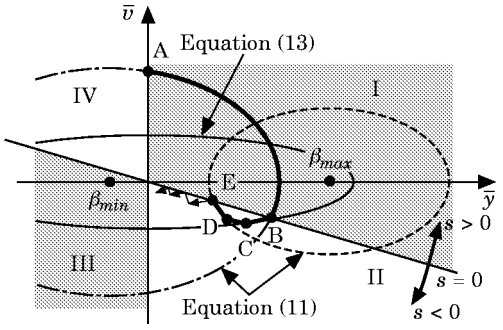

Figure 3. Regions and trajectories in the $\bar{y}$–$\bar{v}$ phase plane.

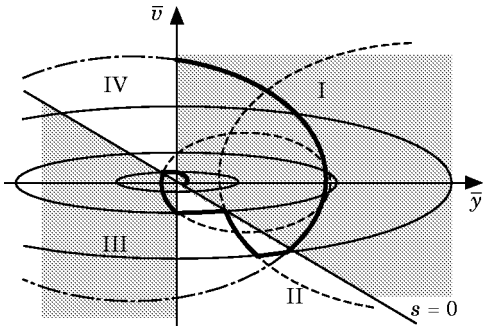

Figure 4. Trajectories in the $\bar{y}$–$\bar{v}$ phase plane.

The solution to motion for cases (A) and (C) is obtained from equation (1):

$$\bar{v}^2 + a^*(\bar{y} - \beta^*)^2 = D^*, \tag{13}$$

where D^* is constant to be determined by the initial condition, and

$$\beta^* = \bar{z} + \bar{F}, \qquad a^* = 4\pi^2. \tag{14}$$

Equation (13) is also the ellipse of which the center β^* moves depending on $\bar{z}$ and $\bar{F}$ in the $\bar{y}$–$\bar{v}$ phase plane. The trajectory when $\bar{F} = 0$ and $\bar{z} = 0$, i.e., the motion for case (A) with no floor excitation, is shown by the thin solid line in Figure 3. The height to width ratio of the ellipse denoted by equation (13) is smaller than the one resulting from equation (11), because the coefficient a^* is smaller than a. The difference is remarkable when v is large.

By switching the elliptic trajectories mentioned above, the motion of mass m is controlled. To this end, we define the switching function:

$$s = \bar{v} + c\bar{y}, \qquad c = \text{constant}. \tag{15}$$

Then the phase plane is divided into four regions, I, II, III and IV, by the switching line $s = 0$ and the vertical line $\bar{y} = 0$, as shown in Figure 3. The trajectory from point A to B in region I is made close to the origin if β is kept as small as possible. This indicates that the joint should be clamped and that the masses m and m_s are stuck holding $\bar{r}_s$ as large as possible. When the trajectory reaches the switching line at point B, the joint is unclamped. Then the trajectory moves from the point B to C in region II, and in the meantime masses m and m_s move independently of each other and the relative displacement $\bar{r}$ varies. When $\bar{r}$ reaches the vicinity of minimum (i.e., maximum β) at point C, the joint is clamped again. Then, after a short duration of slip between points C and D, the masses m and m_s are stuck again and the trajectory moves from point D to E. When the trajectory reaches the switching line at point E, the joint is unclamped again, and the procedure mentioned above is repeated hereafter. As a result, the trajectory converges to the origin fluctuating in the vicinity of the switching line in region II. In regions III and IV, the joint is controlled in the same manner as in regions I and II, taking into account the differences of the signs of $\bar{y}$ and $\bar{v}$. This idea is based on VSS theory. It is known that the behavior of the system when the trajectory moves along the switching line $s = 0$ is given by $\bar{y} = Y \exp(-c\tau)$, where Y is constant [12]. This indicates that $\bar{y}$ simply decreases if $c > 0$, and the decay rate increases with c. However, the trajectory may move to regions III and IV, as shown in Figure 4, when c becomes large, because in practice the trajectory does not remain on the switching line all the time. The trajectory then converges to the origin asymptotically, as will be discussed later in Figures 9 and 13.

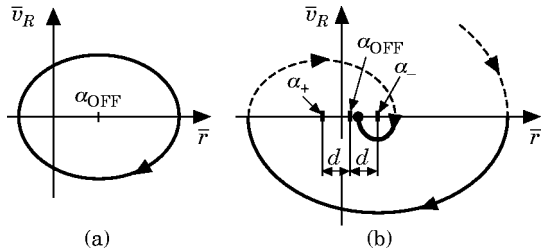

Figure 5. Trajectories in the $\bar{r}$–$\bar{v}_R$ phase plane: (a) joint unclamped; (b) joint clamped.

An important consideration of the procedure is the control of $\bar{r}$. We can follow this precisely by solving equation (2):

$$\bar{v}_R^2 + a_R(\bar{r} - \alpha)^2 = D_R, \tag{16}$$

where D_R is constant and

$$\bar{v}_R = \mathrm{d}\bar{r}/\mathrm{d}\tau, \qquad \alpha = (\bar{y} - \bar{z})(1 - v^2)/v^2 - \bar{F}(1 + 1/\lambda)/v^2, \qquad a_R = 4\pi^2 v^2. \tag{17}$$

Equation (16) indicates an ellipse, the center co-ordinate α of which moves depending on $\bar{y}$, $\bar{z}$ and $\bar{F}$ in the $\bar{r}$–$\bar{v}_R$ phase plane. It is noted that $\bar{F} = 0$ when the joint is unclamped, and that $\bar{F} = \bar{F}_s$ or $-\bar{F}_s$ during slip when the joint is clamped. α is dominated by $\bar{F}$ if $\bar{F}_s$ is much larger than the variation of $\bar{y}$ and $\bar{z}$. Here, we set

$$\alpha \equiv \alpha_{\mathrm{OFF}} = (\bar{y} - \bar{z})(1 - v^2)/v^2 \tag{18}$$

when the joint is unclamped. Then, the trajectory is represented by the single ellipse with a center co-ordinate $\bar{r} = \alpha_{\mathrm{OFF}}$ that shifts depending on $\bar{y}$ and $\bar{z}$, as shown in Figure 5(a). On the other hand, we set

$$\alpha \equiv \alpha_+ = \alpha_{\mathrm{OFF}} - d \quad \text{for } \bar{v}_R > 0, \qquad \alpha \equiv \alpha_- = \alpha_{\mathrm{OFF}} + d \quad \text{for } \bar{v}_R < 0, \tag{19}$$

during slip when the joint is clamped, where

$$d = \bar{F}_s(1 + 1/\lambda)/v^2. \tag{20}$$

In this case, the trajectory is a combination of two families of ellipses, as shown in Figure 5(b) by the broken and solid lines, that have center co-ordinates $r = \alpha_+$ and α_- when $\bar{v}_R > 0$ and $\bar{v}_R < 0$, respectively. It is noted that sticking occurs when the trajectory reaches $\bar{v}_R = 0$ within the region $\alpha_+ < \bar{r} < \alpha_-$, and the relative displacement holds the constant value $\bar{r}_s$

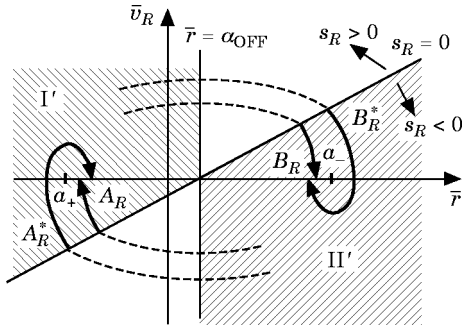

Figure 6. Regions and trajectories in the $\bar{r}$–$\bar{v}_R$ phase plane. ----, Unclamped; ——, clamped.

thereafter. The value of $\bar{r}_s$ depends on the state of motion at the moment at which the joint is clamped. In order to control $\bar{r}_s$, we define the switching function

$$s_R = \bar{v}_R - c_R(\bar{r} - \alpha_{\mathrm{OFF}}), \qquad c_R = \text{constant}. \tag{21}$$

The $\bar{r}$–$\bar{v}_R$ phase plane is divided into four regions by the switching line $s_R = 0$ and the vertical line $\bar{r} = \alpha_{\mathrm{OFF}}$, as shown in Figure 6. When the joint is clamped in region I′, the trajectory moves along the curve A_R or A_R^* during interfacial slip, and then $\bar{r}$ $(=\bar{r}_s)$ is kept to a minimum at $\bar{v}_R = 0$ due to friction. On the other hand, when the joint is clamped in region II′, the trajectory moves along the curve B_R or B_R^*, and then $\bar{r}_s$ is kept to a maximum at $\bar{v}_R = 0$. It is noted that the joint is clamped before $\bar{r}$ reaches its peak when $c_R > 0$. Furthermore, it is possible to clamp the joint after $\bar{r}$ has passed the peak by setting $c_R < 0$. During this process over a finite duration of slip, the energy is dissipated due to the friction force. The duration of slip and the energy dissipation increase with the absolute value of c_R, as will be shown later in Figure 8.

Thus, the joint switching control law is described by means of the hierarchy of the state of $\bar{y}$, $\bar{v}$, $\bar{r}$ and $\bar{v}_R$:

[The state point $(\bar{y}, \bar{v})$ is in region I or region IV of the $\bar{y}$–$\bar{v}$ phase plane]
The joint is clamped if $\beta < \bar{y}$ and the state point $(\bar{r}, \bar{v}_R)$ is in region II′ of the $\bar{r}$–$\bar{v}_R$ phase plane.

[The state point $(\bar{y}, \bar{v})$ is in region II or region III of the $\bar{y}$–$\bar{v}$ phase plane]
The joint is clamped if $\beta > \bar{y}$ and the state point $(\bar{r}, \bar{v}_R)$ is in region I′ of the $\bar{r}$–$\bar{v}_R$ phase plane.

If these conditions are not satisfied, the joint is unclamped so that $\bar{r}$ may vary, and clamped at the moment at which the condition is met.

4. NUMERICAL SIMULATION PROCEDURE

In order to obtain the time history of response, we introduce the state variables

$$x_1 = \bar{y}, \qquad x_2 = \bar{r}, \qquad x_3 = \bar{v}, \qquad x_4 = \bar{v}_R. \tag{22}$$

Equations (1) and (2) are then combined into state form as

$$\mathrm{d}\mathbf{X}/\mathrm{d}\tau = \mathbf{A}_c\mathbf{X} + \mathbf{B}_c\bar{F} + \mathbf{C}_c\bar{z}, \tag{23}$$

where

$$\mathbf{X} = [x_1, x_2, x_3, x_4]^{\mathrm{T}},$$

$$\mathbf{A}_c = \begin{bmatrix} 0, & 0, & 1, & 0 \\ 0, & 0, & 0, & 1 \\ -4\pi^2, & 0, & 0, & 0 \\ 4\pi^2(1 - v^2), & -4\pi^2 v^2, & 0, & 0 \end{bmatrix},$$

$$\mathbf{B}_c = [0, 0, 4\pi^2, -4\pi^2(1 + 1/\lambda)]^{\mathrm{T}}, \qquad \mathbf{C}_c = [0, 0, 4\pi^2, -4\pi^2(1 - v^2)]^{\mathrm{T}}. \tag{24}$$

From the solution of equation (23), we have the state difference equation for the time interval T between times τ_i and τ_{i+1}:

$$\mathbf{X}(i + 1) = \mathbf{A}\mathbf{X}(i) + \mathbf{B}\bar{F}(i) + \mathbf{C}\bar{z}(i), \qquad i = 0, 1, 2, \ldots, \tag{25}$$

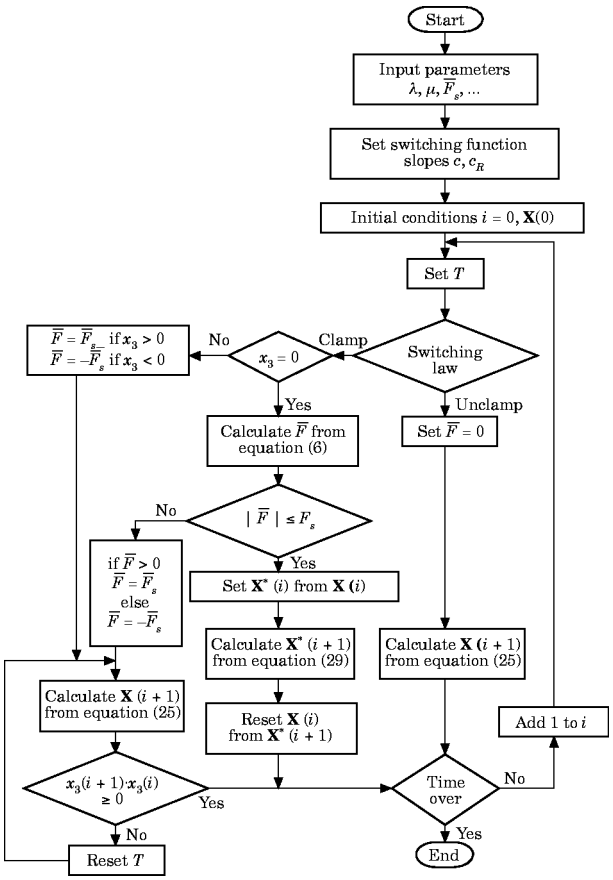

Figure 7. The flowchart of the numerical simulation.

where $\mathbf{X}(i)$, $\bar{F}(i)$ and $\bar{z}(i)$ are the values of $\mathbf{X}$, $\bar{F}$ and $\bar{z}$ at time $\tau_i = iT$, respectively, and

$$\mathbf{A} = \exp(\mathbf{A}_c T), \qquad \mathbf{B} = (\mathbf{A} - \mathbf{I})\mathbf{A}_c^{-1}\mathbf{B}_c, \qquad \mathbf{C} = (\mathbf{A} - \mathbf{I})\mathbf{A}_c^{-1}\mathbf{C}_c \tag{26}$$

and $\mathbf{I}$ is the unit matrix. The time history, when the joint is unclamped or when the joint is clamped and interfacial slip occurs, is calculated from equation (25) by setting $\bar{F} = 0$, $\bar{F}_s$ or $-\bar{F}_s$.

On the other hand the state equation when the joint is clamped and touching is obtained from equation (5):

$$\mathrm{d}\mathbf{X}^*/\mathrm{d}\tau = \mathbf{A}_c^*\mathbf{X}^* + \mathbf{B}_c^* x_2^* + \mathbf{C}_c^* \bar{z}, \tag{27}$$

where

$$\mathbf{X}^* = [x_1, x_3]^{\mathrm{T}}, \qquad \mathbf{A}_c^* = \begin{bmatrix} 0, & 1 \\ -4\pi^2(1 + \lambda v^2)/(1 + \lambda), & 0 \end{bmatrix},$$

$$\mathbf{B}_c^* = [0, -4\pi^2\lambda v^2/(1 + \lambda)]^{\mathrm{T}}, \qquad \mathbf{C}_c^* = [0, 4\pi^2(1 + \lambda v^2)/(1 + \lambda)]^{\mathrm{T}}. \tag{28}$$

It is noted that $x_4 = 0$ and that x_2^* is the value of x_2 at the moment the joint interface is touching. The state difference equation for this case is also obtained as

$$\mathbf{X}^*(i + 1) = \mathbf{A}^*\mathbf{X}^*(i) + \mathbf{B}^* x_2^* + \mathbf{C}^* \bar{z}(i), \tag{29}$$

where

$$\mathbf{A}^* = \exp(\mathbf{A}_c^* T), \qquad \mathbf{B}^* = (\mathbf{A}^* - \mathbf{I})(\mathbf{A}_c^*)^{-1}\mathbf{B}_c^*, \qquad \mathbf{C}^* = (\mathbf{A}^* - \mathbf{I})(\mathbf{A}_c^*)^{-1}\mathbf{C}_c^*. \quad (30)$$

By specifying the initial conditions, the $\mathbf{X}(i)$'s are obtained iteratively by applying equation (25) or equation (29) which are changed according to the switching control law. The flowchart of the numerical simulation is shown in Figure 7. Note that a computational error is caused if the time when the interface starts to touch is not taken into consideration accurately. This time is checked by varying the time interval T when the sign of relative velocity x_3 changes.

5. NUMERICAL EXAMPLES FOR TRANSIENT RESPONSE

Numerical examples are presented to demonstrate the effectiveness and performance of the method proposed in this paper. The following numerical values are used for the system parameters unless otherwise stated: $\lambda = 0{\cdot}01$, $v = 20$, $c = 10$, $c_R = 200$, $\bar{F}_s = 2$. In order to investigate the transient response under no floor excitation ($\bar{z} = 0$), the initial conditions are given as $\bar{y} = 0$, $\bar{v} = 5$, $\bar{r} = 0$ and $\bar{v}_R = 0$. In Figures 8(a) and 8(b) are shown the displacement transient responses and the energy time histories for various values of c_R. The displacement $\bar{y}$ is monotonic decay with no oscillation and is hardly influenced by c_R, while the relative displacement $\bar{r}$ is decaying oscillation, the decay of which increases as c_R leaves zero. It is noted that $\bar{r}$ is kept constant after it has passed the peak for $c_R = -100$ and -40, as discussed in Figure 6, as it relates to equation (21). The total energy consists of the energies of the m–k_a and m_s–k_s systems, and the time histories are normalized with the initial total energy. It is shown that the energy of the m–k_a system diminishes rapidly and is almost independent of c_R, while the energy of the m_s–k_s system dominates the total

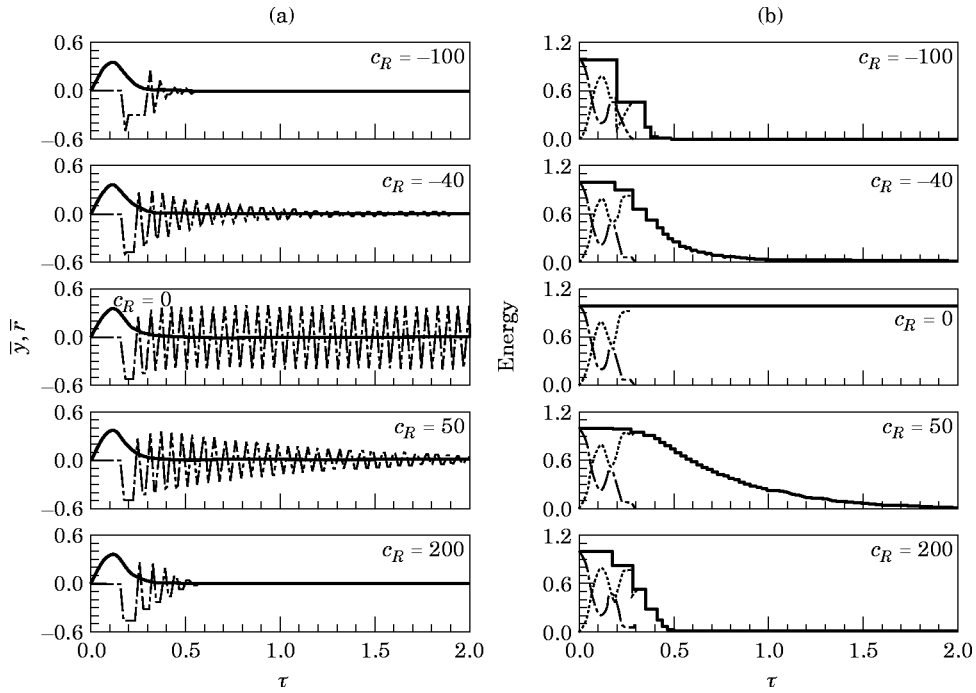

Figure 8. (a) The displacement transient response for various values of c_R. ——, $\bar{y}$; —·—, $\bar{r}$. (b) The energy time history for various values of c_R. ——, Total; —·—, m–k_a system; ----, m_s–k_s system.

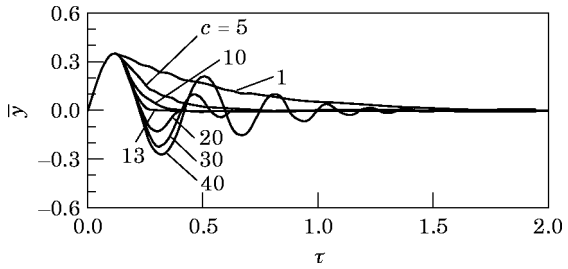

Figure 9. The displacement transient response for various values of c.

energy after the energy of the m–k_a system has diminished, and varies depending on c_R. This indicates that the vibration of main mass m is suppressed even if the total energy is not dissipated. Note that the slip and energy dissipation do not occur for $c_R = 0$, because the relative velocity $\bar{v}_R = 0$ at the moment at which the joint is clamped. Transient responses of $\bar{y}$ for various values of c are shown in Figure 9. The responses for $c < 13$ are monotonic decay, while those for $c > 20$ are oscillatory decay. It is noted that $\bar{y}$ reduces most rapidly in the vicinity of c where the type of response changes. These types of motion are made clear by considering the phase plane trajectory, as discussed in Figures 3 and 4. The type of motion changes depending on the stiffness ratio v, as will also be discussed later in Figure 13. The slope c of the switching line corresponds to the time lag from the instant of peak displacement for actuating the control as suggested by Warkentin and Semercigil [14].

In order to evaluate the control performance for the transient response, we introduce the following performance indices:

$$G_y = \left(\int_0^{T_E} |\bar{y}|\tau \, \mathrm{d}\tau\right) \Big/ \left(T_E \int_0^{T_E} |\bar{y}| \, \mathrm{d}\tau\right),$$

$$G_R = \left(\int_0^{T_E} |\bar{r}|\tau \, \mathrm{d}\tau\right) \Big/ \left(T_E \int_0^{T_E} |\bar{r}| \, \mathrm{d}\tau\right), \qquad A_y = \left(\int_0^{T_E} \bar{y} \, \mathrm{d}\tau\right) \Big/ \left(\int_0^{T_E} |\bar{y}| \, \mathrm{d}\tau\right). \tag{31}$$

The indices G_y and G_R are defined as the centroidal co-ordinates of the area under the absolute response curves $|\bar{y}|$ and $|\bar{r}|$ between times $\tau = 0$ and $\tau = T_E$, respectively, and normalized with T_E. They represent decay properties of $\bar{y}$ and $\bar{r}$, since they are small for rapid decay and reach 0·5 for no decay. The index A_y is defined as the ratio of the area surrounded by the response curve $\bar{y}$ and horizontal line $\bar{y} = 0$ to the area under the absolute response curve $|\bar{y}|$ between $\tau = 0$ and $\tau = T_E$. The type of response $\bar{y}$ is understood

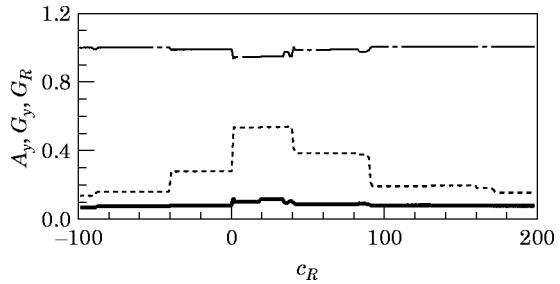

Figure 10. The variation of A_y, G_y and G_R versus c_R. —·—, A_y;—— , G_y; ----, G_R.

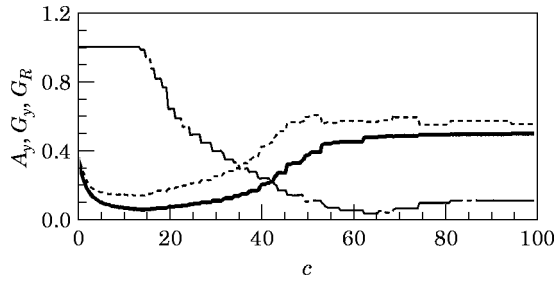

Figure 11. The variation of A_y, G_y and G_R versus c. — - —, A_y; ——, G_y; - - - -, G_R.

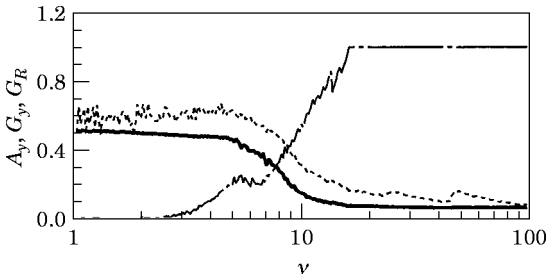

Figure 12. The variation of A_y, G_y and G_R versus v. — - —, A_y; ——, G_y; - - - -, G_R.

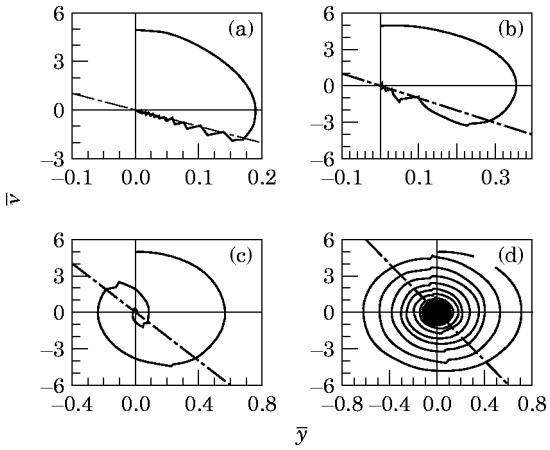

Figure 13. The phase plane trajectory of $\bar{y}$: (a) $v = 50$; (b) $v = 20$; (c) $v = 10$; (d) $v = 5$. ——, Trajectory; — - —, switching line ($s = 0$).

by the index A_y, since $A_y = 1$ if $\bar{y}$ decays monotonically without changing sign, while $A_y = 0$ if $\bar{y}$ oscillates with constant amplitude.

The effect of c_R on the performance indices is shown in Figure 10. It is observed that G_y and A_y remain constant near 0 and 1 for all of the region of c_R, respectively, while G_R is large in the region $-40 < c_R < 90$. These results coincide with the result of Figure 8(a). The effect of c on the performance indices is shown in Figure 11. It is shown that $A_y = 1$ for $c < 13$ and it decreases with increasing c in the region $c > 13$, and G_y reaches a minimum in the vicinity of $c = 13$. These results precisely indicate the characteristic of displacements shown in Figure 9. Furthermore, we can see that $\bar{y}$ oscillates with no decay for $c > 50$ because G_y reaches 0·5 and A_y is almost zero in that region. The effect of the stiffness ratio v on the performance indices is shown in Figure 12. The displacements $\bar{y}$

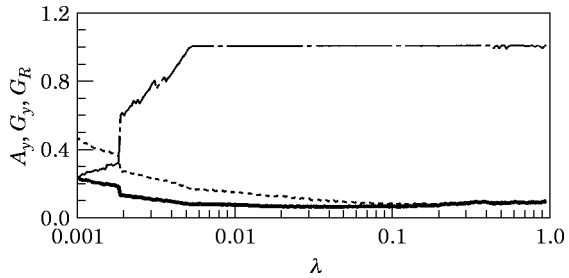

Figure 14. The variation of A_y, G_y and G_R versus λ. —·—, A_y; ——, G_y; ----, G_R.

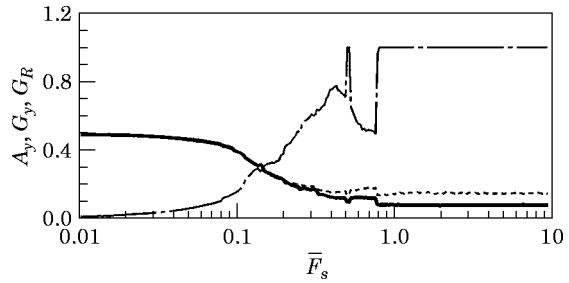

Figure 15. The variation of A_y, G_y and G_R versus $\bar{F}_s$. —·—, A_y; ——, G_y; ----, G_R.

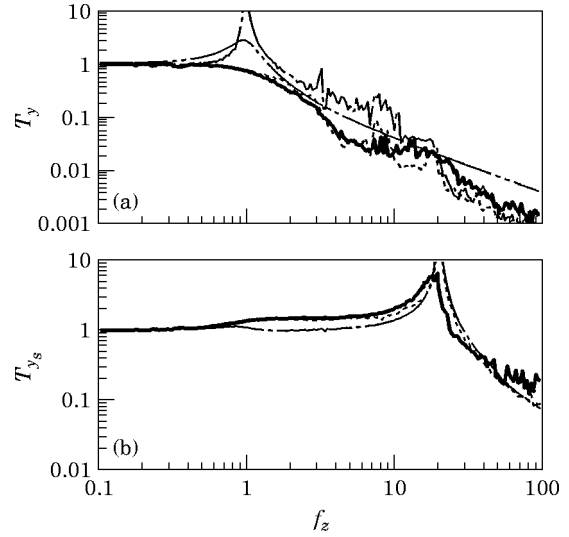

Figure 16. (a) Transmissibility T_y for various $\bar{F}_s$: —·—, $\bar{F}_s = 0{\cdot}1$, ----, 0·5; ——, 2·0; —··—, passive ($\zeta = 0{\cdot}2$). (b) Transmissibility T_{ys} for various $\bar{F}_s$; —·—, $\bar{F}_s = 0{\cdot}1$; ----, 0·5;—— , 2·0.

and $\bar{r}$ are effectively suppressed for $v > 11$ where G_y and G_R are small. We also see that $\bar{y}$ decays monotonically for $v > 15$, where $A_y = 1$. The characteristics of the present method are clarified by the trajectories in the $\bar{y}$–$\bar{v}$ phase plane, as shown in Figure 13 for $v = 5$, 10, 20 and 50. The trajectory for $v = 50$ is trapped on the switching line $s = 0$ and converges to the origin in the same manner as the sliding mode of VSS. As a result, $\bar{y}$ decays monotonically. This feature is remarkable when the switching interval is short. Note that

the switching interval depends on the time duration in which β moves between β_{min} and β_{max} when the joint is unclamped, as discussed in Figure 3, and is determined by the period of the m_s–k_s system. The stiffness v defined in equation (9) originally indicates the ratio between the natural frequencies of the m_s–k_s and m–k_a systems. As a result, the switching interval depends on v. This switching interval corresponds to the control duration suggested by Warkentin and Semercigil [14]. With decreasing v, the switching interval increases and the trajectory leaves the switching line. Then, the trajectory spirals into the origin showing oscillatory decay of $\bar{y}$ as for cases $v = 5$ and $v = 10$. The effect of mass ratio $\lambda = m_s/m$ on the performance indices is shown in Figure 14. The performance declines with decreasing λ, because the spring stiffness k_s, becomes small for small mass m_s under constant stiffness ratio $v^2 = (k_s/m_s)/\Omega_0^2$. In general, the auxiliary mass m_s, i.e., λ, should be set as small as possible in order to save the space and cost of the system. The effect of the friction force $\bar{F}_s$ is shown in Figure 15. The non-dimensional parameter $\bar{F}_s$ is the ratio between the magnitude of friction force and the force that is needed to support mass m under gravitation. The vibration is not reduced for $\bar{F}_s < 0{\cdot}1$ because there is no touching and the proposed control logic does not hold when $\bar{F}_s$ is small. It is also desirable to set $\bar{F}_s$ as small as possible, in order to save the power of the brake device.

6. NUMERICAL EXAMPLES FOR DISPLACEMENT TRANSMISSIBILITY

The vibration isolation performance is investigated by the displacement transmissibility ratio when the floor is subject to the harmonic displacement excitation $\bar{z} = Z_{amp} \sin(2\pi f_z \tau)$, where Z_{amp} is the amplitude and f_z is the frequency. The displacement transmissibility ratios T_y and T_{ys} are defined by $T_y = (\bar{y})_{rms}/(\bar{z})_{rms}$ and $T_{ys} = (\bar{y}_s)_{rms}/(\bar{z})_{rms}$, where $(\bar{y})_{rms}$, $(\bar{y}_s)_{rms}$ and $(\bar{z})_{rms}$ are the root mean square (r.m.s.) of displacements $\bar{y}$, $\bar{y}_s$ and $\bar{z}$, respectively. The system parameters denoted in the previous section are used unless otherwise stated, and initial conditions of the masses are set at zero. In Figures 16(a) and 16(b) are shown the transmissibilities T_y and T_{ys} versus f_z with $Z_{amp} = 0{\cdot}2$ for various values of $\bar{F}_s$, respectively. The transmissibility of the passive m–k_a system with damping ratio $\zeta = 0{\cdot}2$ is also shown in Figure 16(a). Although the transmissibility for $\bar{F}_s = 0{\cdot}1$ becomes large in the vicinity of

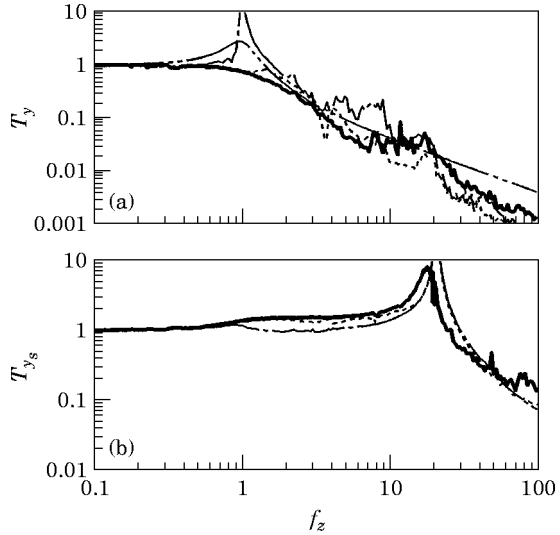

Figure 17. (a) Transmissibility T_y for various Z_{amp}: ——, $Z_{amp} = 0{\cdot}1$; ----, 1·0; —·—, 3·0; —··—, passive ($\zeta = 0{\cdot}2$). (b) Transmissibility T_{ys} for various Z_{amp}: ——, $Z_{amp} = 0{\cdot}1$; ----, 1·0; —·—, 3·0.

the non-dimensional natural frequency of the m–k_a system ($f_z = 1$), those for $\bar{F}_s = 0{\cdot}5$ and $\bar{F}_s = 2{\cdot}0$ have no peak and decrease with an increase in f_z. Thus, the main mass m is isolated from the floor excitation for $\bar{F}_s > 0{\cdot}5$ and $f_z > 1$. It is noted that, in practice, the natural frequency of the m–k_a system can be set as small as required by decreasing the stiffness k_a without degenerating the transient response and static stability, because they are compensated by the auxiliary stiffness k_s if k_s is set large. The transmissibility T_{ys} gradually increases with increasing f_z and becomes large in the vicinity of the non-dimensional natural frequency of the m_s–k_s system, $f_z = 20$. This frequency corresponds to the parameter $v = 20$, as mentioned in Figure 13. Thus the vibration of auxiliary mass m_s is amplified, but the excess vibration is avoided for $\bar{F}_s > 2{\cdot}0$. The transmissibility ratios T_y and T_{ys} for the floor amplitudes $Z_{amp} = 0{\cdot}1$, 1 and 3, with $\bar{F}_s = 2$, are shown in Figures 17(a) and 17(b) respectively. The transmissibilities have large resonant peaks for large Z_{amp}. This peak is improved by increasing the friction force $\bar{F}_s$.

7. CONCLUSIONS

This paper presents a new method to isolate and reduce the vibration by on–off control of the friction force at the auxiliary spring support. The switching control law is deduced from the VSS theory. In the numerical simulations, it is shown that the energy dissipation due to friction is controlled by the slope c_R of switching line in the phase plane of relative displacement and velocity. Furthermore, it is found that the energy of the main system is reduced even if the total energy is not dissipated, because energy is transferred to the auxiliary system. It is also shown that the motion of the main mass for the transient response is classified into monotonic decay similar to the VSS sliding mode and oscillatory decay. This type of motion depends on the slope c of the switching line in the phase plane of the main mass displacement and velocity, and it is found that the main mass displacement decreases most rapidly in the vicinity of c where the type of motion changes. The effects of the mass ratio λ, the frequency ratio v and the friction force $\bar{F}_s$ on the transient response are investigated and shown by the performance indices. The numerical results for the displacement transmissibility confirm high vibration isolation performance with no resonant peaks.

REFERENCES

1. D. Karnopp, M. J. Crosby and R. A. Harwood 1974 *Transactions of the American Society of Mechanical Engineers*, *Journal of Engineering for Industry* **96**(2), 619–626. Vibration control using semi-active force generators.
2. D. Hrovat, D. L. Margolis and M. Hubbard 1988 *Transactions of the American Society of Mechanical Engineers*, *Journal of Dynamic Systems*, *Measurement*, *and Control* **110**(3), 288–296. An approach toward the optimal semi-active suspension.
3. D. Karnopp 1990 *Transactions of the American Society of Mechanical Engineers*, *Journal of Dynamic Systems*, *Measurement*, *and Control* **112**(3), 448–455. Design principles for vibration control systems using semi-active dampers.
4. J. Lieh 1993 *Transactions of the American Society of Mechanical Engineers*, *Journal of Vibration and Acoustics* **115**(3), 340–343. Semiactive damping control of vibrations in automobiles.
5. A. A. Ferri and B. S. Heck 1992 *Journal of Guidance*, *Control*, *and Dynamics* **15**(5), 1258–1264. Analytical investigation of damping enhancement using active and passive structural joints.
6. J. C. Chen 1984 *Journal of Spacecraft and Rockets* **21**(5), 463–467. Response of large space structures with stiffness control.
7. M. S. Habib and C. J. Radcliffe 1991 *Transactions of the American Society of Mechanical Engineers*, *Journal of Dynamic Systems*, *Measurement*, *and Control* **113**(2), 295–299. Active parametric damping of distributed parameter beam transverse vibration.
8. C. D. Rahn and C. D. Mote Jr. 1994 *Transactions of the American Society of Mechanical*

Engineers, *Journal of Vibration and Acoustics* **116**(3), 379–385. Parametric control of flexible systems.
9. H. Yamaguchi, S. Shioya and M. Oda 1995 *Proceedings of the ASME/JSME Pressure Vessel and Piping Conference*, *Seismic Engineering*, *Hawaii*, *July*, PVP-Vol. **312**, 399–404. Vibration isolation and reduction by spring-stiffness control based on theory of variable structure systems.
10. V. I. Utkin 1977 *IEEE Transactions on Automatic Control* **AC-22**(2), 212–222. Variable structure systems with sliding modes.
11. K. D. Young 1987 *IEEE Transactions on Systems*, *Man*, *and Cybernetics* **SMC-8**(2), 101–109. Controller design for a manipulator using theory of variable structure systems.
12. F. Harashima and H. Hashimoto 1985 *Systems and Control* **29**(2), 94–103. Sliding mode and its application—I (in Japanese).
13. J. Onoda, T. Endo, H. Tamaoki and N. Watanabe 1991 *American Institute of Aeronautics and Astronautics Journal* **29**(6), 977–983. Vibration suppression by variable-stiffness members.
14. A. Warkentin and S. E. Semercigil 1995 *Journal of Sound and Vibration* **187**, 1–21. Variable stiffness control of a single-link flexible robotic arm.

APPENDIX: NOMENCLATURE

A_y	performance index that indicates the type of main mass response
c	slope of the switching line in the $\bar{y}$–$\bar{v}$ phase plane
c_R	slope of the switching line in the $\bar{r}$–$\bar{v}_R$ phase plane
f_z	frequency of the floor harmonic displacement excitation
F_s, $\bar{F}_s$	magnitude of the constant friction force during slip
G_R	performance index that indicates the decay property of $\bar{r}$
G_y	performance index that indicates the decay property of $\bar{y}$
k_a	stiffness of the main spring
k_s	stiffness of the auxiliary spring
m	mass of the main object to be reduced by vibration
m_s	mass of the auxiliary joint switching device
r, $\bar{r}$	relative displacement between the main and auxiliary masses
r_s, $\bar{r}_s$	relative displacement at the moment the main and auxiliary masses are touching
s	switching function in the $\bar{y}$–$\bar{v}$ phase plane
s_R	switching function in the $\bar{r}$–$\bar{v}_R$ phase plane
t, τ	time
T_y	displacement transmissibility of the main mass
T_{ys}	displacement transmissibility of the auxiliary mass
$\bar{v}$	velocity of the main mass
$\bar{v}_R$	relative velocity
y, $\bar{y}$	displacement of the main mass
y_s	displacement of the auxiliary mass
z, $\bar{z}$	displacement of the floor
λ	mass ratio
v	stiffness ratio